RSC Advances

PAPER

View Article Online
View Journal | View Issue

Cite this: *RSC Adv.*, 2026, **16**, 29905

Pentacyclic triterpenoids from *Ziziphus jujuba* Lamk. fruits as dual inhibitors of PTP1B and α-glucosidase: *in vitro* and *in silico* evaluations

Linh Tran,[abd] Thanh-Tung Phan,[cd] Le Viet Ha Tran,[e] Minh Canh Nguyen,[ad] Huu Canh Vo,[ad] Nguyen Tri Quang,[f] Phuc Tran Huu Le,[g] Quang-Minh Mai,[abd] Khac-Minh Thai[abd] and Huynh Nguyen Khanh Tran *[abd]

Ziziphus jujuba Lamk. (Táo Ta) is widely used in traditional Asian medicine as a superfruit. An ethanol extract of the *Z. jujuba* fruit exhibited remarkable inhibition against PTP1B and was isolated *via* bioassay-guided fractionation, resulting in the identification of fifteen active triterpenoids (**1–15**), namely, betulinic acid (**1**), corosolic acid (**2**), oleanolic acid (**3**), alphitolic acid (**4**), maslinic acid (**5**), 3-*O*-*cis*-*p*-coumaroyl alphitolic acid (**6**), 3-*O*-*trans*-*p*-coumaroyl alphitolic acid (**7**), 2-*O*-*trans*-*p*-coumaroyl alphitolic acid (**8**), 2-*O*-*cis*-*p*-coumaroyl alphitolic acid (**9**), ceanothic acid (**10**), zizyberanalic acid (**11**), *trans*-*p*-coumaroyl betulinic acid (**12**), betulonic acid (**13**), ursolic acid (**14**), and oleanonic acid (**15**). Their chemical structures were identified using nuclear magnetic resonance (NMR) spectroscopy and compared with those reported in other papers. Among the compounds tested for their effect against PTP1B and α-glucosidase, compounds **1–3** displayed the most potent inhibitory activity, with their IC_{50} values ranging from 6.75 to 17.02 μM. Besides, compounds **4**, **10**, and **13** exhibited weak PTP1B inhibitory activity (IC_{50} = 53.42 to 90.90 μM), while **5–15** showed no inhibitory effect at all tested concentrations. Additionally, molecular docking and molecular dynamics simulations were performed to evaluate the binding affinity of compounds **1–3** toward PTP1B and α-glucosidase, two key enzymes involved in glucose homeostasis. These interactions may contribute to the modulation of insulin signaling pathways and postprandial glucose levels, thereby improving glycemic control in diabetes. Moreover, *in silico* ADME and toxicity prediction further suggested that **1–3** possessed favorable pharmacokinetic properties and lower predicted toxicity. These findings provide a rational basis for using *Ziziphus* sourced from Vietnam to develop potential PTP1B and α-glucosidase dual inhibitors, warranting further investigations, and are considered the first report on the chemical and bioactive investigation of this species.

Received 31st March 2026
Accepted 18th May 2026

DOI: 10.1039/d6ra02679f

rsc.li/rsc-advances

Introduction

In traditional medicine, fruits of the *Ziziphus* genus have been widely used to treat various ailments, including digestive disorders,[1] general weakness, liver diseases, obesity, urinary problems,[2] diabetes, skin infections, loss of appetite, fever, pharyngitis, bronchitis, anemia, diarrhea, insomnia, and certain types of cancer.[1] Recent pharmacological studies have demonstrated that extracts from the *Ziziphus* species possess multiple biological activities,[1,3] including anti-tumor,[4] antioxidant,[5] anti-inflammatory,[6] and hepatoprotective effects,[7] with their activity reported against various cancer cell lines.[8] Nevertheless, the investigation of the chemical constituents of *Z. jujuba* Lamk. and its anti-diabetic and signaling pathways have not yet been reported.

Pentacyclic triterpenoids are naturally occurring compounds featuring a five-ring carbon skeleton, commonly found in medicinal plant sources.[9] Among them, oleanolic acid, classified under the oleanane type, is one of the most studied molecules due to its demonstrated ability to inhibit protein tyrosine phosphatase 1B and α-glucosidase,[10] the key negative regulator of insulin signaling and glycemic control in diabetes. Recent research has shown that the PTP1B inhibition by oleanolic acid and its derivatives can enhance insulin sensitivity, promote hepatic glycogen synthesis, modulate leptin/ghrelin levels,

[a]*Faculty of Pharmacy, University of Health Sciences, Ho Chi Minh City, Vietnam. E-mail: thnkhanh@uhsvnu.edu.vn; Tel: +84 939775593*
[b]*Research Center for Discovery and Development of Healthcare Products, Vietnam National University Ho Chi Minh City, Ho Chi Minh City, Vietnam*
[c]*Faculty of Chemistry, University of Science, Ho Chi Minh City 70000, Vietnam*
[d]*Vietnam National University, Ho Chi Minh City 70000, Vietnam*
[e]*Faculty of Traditional Medicine, University of Medicine and Pharmacy at Ho Chi Minh City, Vietnam*
[f]*College of Natural Sciences, Can Tho University, 3/2 Street, Can Tho 900000, Vietnam*
[g]*FPT University, Greenwich Vietnam, Hochiminh Campus, Ho Chi Minh City, Vietnam*

reduce serum glucose, and act on signaling pathways, such as PPARs, AMPK, or AKT.[10] Structurally, the critical features of pentacyclic triterpenoids, such as the hydroxyl group at C-2, 3; the double bond at C-12, 13, 20, and 29; and the free carboxylic acid at C-28, are essential for the vigorous binding and inhibitory activity against PTP1B. Additionally, SAR studies have demonstrated that the glycoside substitutions and modifications of the C-28 acidic chain can significantly improve water solubility and inhibitory potency. Besides oleanolic acid, other pentacyclic triterpenoids, such as ursolic acid, corosolic acid, and betulinic acid, have also shown potential in modulating glucose metabolism through PTP1B inhibition and related pathways.[11]

Although *Z. jujuba* has been extensively investigated, previous studies have primarily focused on cultivated or processed materials, often reported under the name *Z. jujuba* var. *inermis* (Táu tàu). In contrast, the phytochemical composition and biological potential of Vietnamese *Z. jujuba* Lamk. fruits (Táo ta) remain insufficiently explored, particularly in the context of dual-target antidiabetic activity. Although several pentacyclic triterpenoids have previously been reported as PTP1B or α-glucosidase inhibitors, studies systematically evaluating the dual inhibitory potential of triterpenoids from Vietnamese *Z. jujuba* Lamk. fruits remain limited. In addition, the comparative bioactivity assessment of multiple triterpenoid subclasses under the same experimental conditions has rarely been reported. Therefore, the present study represents the first comprehensive phytochemical and bioactivity investigation of Vietnamese *Z. jujuba* Lamk., including the comparative evaluation of fifteen triterpenoids in a single experimental system. Furthermore, this study provides new bioactivity information for several less-studied compounds and offers valuable insights into the structure–activity relationships of naturally occurring pentacyclic triterpenoids. Building on these insights, our research focuses on the bioactive-guided isolation of targeted pentacyclic triterpenoids, including betulinic acid (**1**), corosolic acid (**2**), oleanolic acid (**3**), alphitolic acid (**4**), and maslinic acid (**5**), 3-*O*-*cis*-*p*-coumaroyl alphitolic acid (**6**),[12] 3-*O*-*trans*-*p*-coumaroyl alphitolic acid (**7**),[12] 2-*O*-*trans*-*p*-coumaroyl alphitolic acid (**8**),[12] 2-*O*-*cis*-*p*-coumaroyl alphitolic acid (**9**),[12] ceanothic acid (**10**),[13] zizyberanalic acid (**11**),[14] *trans*-*p*-coumaroyl betulinic acid (**12**),[15] betulonic acid (**13**),[16] ursolic acid (**14**),[17] and 3-*oxo*-oleanolic acid (**15**),[18] and their structures are elucidated by detailed NMR spectroscopic analysis and comparison with reported data. This integrated strategy is expected to identify new PTP1B and α-glucosidase inhibitors from Vietnamese *Z. jujuba* Lamk. fruits, prompting a comprehensive study of their purification techniques, structural characteristics, and bioactivities through *in vitro* assays, molecular docking, molecular dynamics, and *in silico* ADME/toxicity predictions.

Results and discussion

Bioactivity-guided isolation of anti-PTP1B constituents

Based on the inhibitory activity of the EtOH extract and $CHCl_3$ fraction against protein tyrosine phosphatase 1B, a series of chromatographic techniques, including liquid–liquid partitioning, normal-phase (NP) and reversed-phase (RP) column chromatography, Sephadex gel filtration, and preparative HPLC, were performed, leading to the isolation of fifteen triterpenoids (**1–15**) (Fig. 1). Structural elucidation was achieved through the analysis of ^1H and ^{13}C NMR spectra, in combination with comparison to previously reported data, allowing for the identification and assignment of the isolated compounds (Fig. 2).

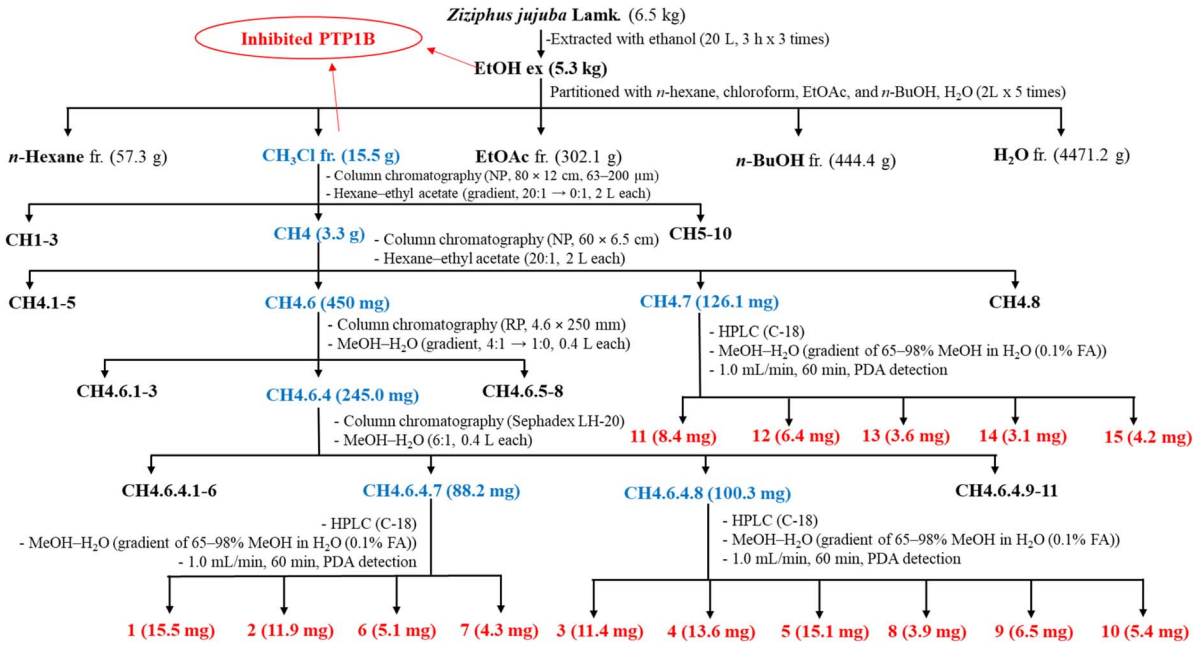

Fig. 1 Bioassay-guided isolation of the compounds **1–15**.

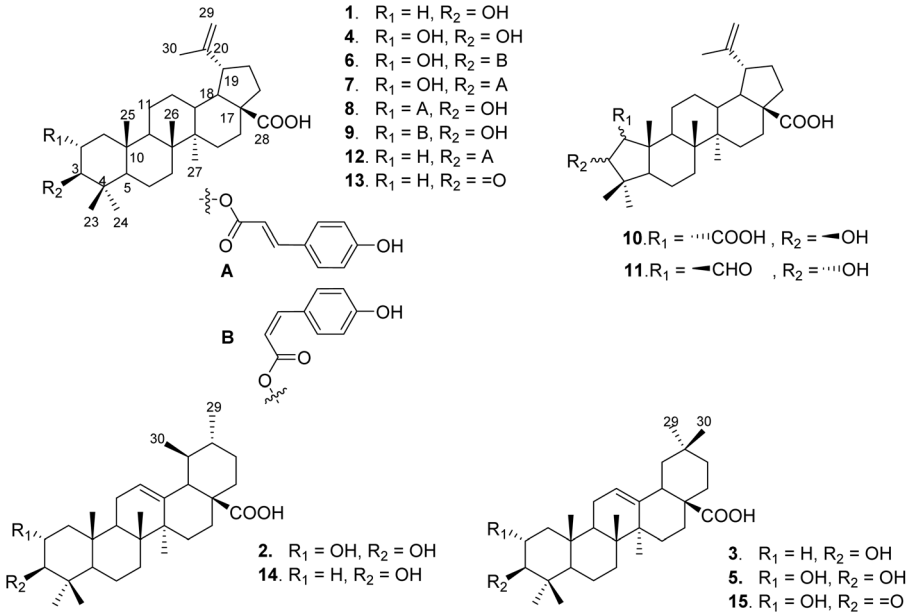

Fig. 2 Chemical structures of the 15 isolated compounds **1–15** from the *Z. jujuba* Lamk. fruit.

Structural elucidation of triterpenoids (1–15)

Compound **1** was isolated as a white amorphous powder. The ^{1}H-NMR spectrum of **1** (Table 1) showed signals for five methyl groups at δ_H 0.86 (3H, s, H-25), 1.04 (3H, s, H-24), 1.09 (s, 3H, H-26), 1.10 (3H, s, H-27), and 1.25 (3H, s, H-23) and a isopropenyl methyl group at δ_H 1.82 (3H, s, H-30), as well as an α-oxymethine proton at δ_H 3.48 (1H, t, J = 8.25 Hz, H-3). In addition, two exo-methylene protons at δ_H 4.97 (1H, brs, H-29b) and 4.80 (1H, brs, H-29a) were observed. The ^{13}C-NMR spectrum (Table 2) showed 30 signals assignable to a carbonyl group at δ_C 179.4 (C-28), an oxygenated carbon at δ_C 78.6 (C-3), and two olefinic carbons at δ_C 151.8 (C-20) and 110.4 (C-29). Based on the above results, compound **1** was identified as betulinic acid by the comparison of spectral data with those in the literature.[19,20]

Compound **2** was obtained as a white amorphous powder. The ^{1}H-NMR spectrum of **2** (Table 1) showed characteristic signals for seven methyl groups at δ_H 1.30 (3H, s, H-23), 1.23 (3H, s, H-26), 1.10 (3H, s, H-27), 1.07 (3H, s, H-24), 1.01 (3H, s, H-25), 0.97 (3H, d, J = 6.0 Hz, H-29) and 1.01 (3H, d, J = 6.3 Hz, H-30); an olefinic proton at δ_H 5.49 (1H, t, J = 3.6 Hz, H-12); and two oxygenated proton signals at δ_H 4.12 (1H, ddd, J = 11.2, 9.3, 4.6 Hz, H-2β) and 3.42 (1H, d, J = 8.1 Hz, H-3α). The ^{13}C-NMR spectra (Table 2) showed 30 signals, including seven methyls at δ_C 30.4 (C-23), 24.2 (C-30), 25.4 (C-27), 19.3 (C-29), 18.2 (C-26), 18.0 (C-24), and 17.4 (C-25) and olefinic carbons at δ_C 139.8 (C-13) and 125.8 (C-12). These spectral data suggested that **2** was a 2,3-dihydroxy-ursan-type triterpenoid. The signals of oxygenated C-2 and 3 were displayed at δ_C 69.0 (C-2) and 84.3 (C-3), which correlated to δ_H 4.12 (1H, ddd, J = 11.2, 9.3, 4.6 Hz, H-2β) and 3.42 (1H, d, J = 8.1 Hz, H-3α) in the 1D-NMR spectrum. Therefore, compound **2** was identified as corosolic acid by comparison with those in the literature.[21,22]

Table 1 ^{1}H-NMR data of the active compounds **1–5** [a]

Position	**1**[a]	**2**[a]	**3**[b]	**4**[a]	**5**[c]
2		4.12 (ddd, 11.2, 9.3, 4.6)		4.11 (td, 10.3, 4.2)	3.58 (ddd, 11.3, 9.6, 4.3)
3	3.48 (t, 8.3)	3.42 (d, 8.1)	3.22 (dd, 11.3, 4.4)	3.41 (d, 9.3)	2.87 (d, 9.6)
12		5.49 (t, 3.6)	5.28 (t, 3.7)		5.22 (t, 3.4)
23	1.25 (s)	1.30 (s)	0.075 (s)	1.06 (m)	0.91 (s)
24	1.04 (s)	1.00 (s)	0.91 (s)	1.28 (s)	0.87 (s)
25	0.86 (s)	1.01 (s)	0.77 (s)	1.06 (m)	0.97 (s)
26	1.09 (s)	1.23 (s)	0.98 (s)	0.91 (s)	0.78 (s)
27	1.10 (s)	1.10 (s)	1.13 (s)	1.06 (m)	1.13 (s)
29	4.97 (brs)	0.97 (d, 6.0)	0.90 (s)	4.94 (s)	0.77 (s)
	4.80 (brs)			4.78 (s)	
30	1.82 (s)	1.01 (d, 6.3)	0.92 (s)	1.79 (s)	0.98 (s)

[a] Measured in pyridine-d_5[a] and chloroform-d[b] in 500 MHz and in methanol-d_4[c] in 400 MHz. δ_H in ppm and J in Hz.

Table 2 ^{13}C-NMR data of the active compounds **1–5** [a]

Position	**1**[a]	**2**[a]	**3**[b]	**4**[a]	**5**[c]
1	39.8	48.4	38.5	48.7	46.9
2	28.8	69.0	27.3	69.3	68.3
3	78.6	84.3	79.2	84.3	83.3
4	40.0	40.3	38.9	40.4	39.4
5	56.4	54.0	55.4	56.5	55.5
6	19.3	21.9	18.4	18.2	18.4
7	35.4	34.0	33.2	35.2	32.7
8	41.6	40.5	39.4	41.6	39.3
9	51.5	48.5	47.8	50.2	48.7
10	38.0	38.9	37.2	39.2	38.1
11	21.7	24.4	23.7	21.8	25.2
12	26.6	125.8	122.8	26.5	122.2
13	39.1	139.8	143.8	39.1	144.2
14	43.4	43.0	41.7	43.4	41.5
15	31.7	29.8	27.8	30.7	27.6
16	33.4	29.1	23.5	33.4	23.4
17	57.1	48.6	46.7	57.1	46.5
18	48.3	56.4	41.1	51.4	41.7
19	50.3	40.0	46.0	48.3	46.1
20	151.8	39.9	30.8	151.8	30.4
21	30.8	31.6	33.9	31.7	33.7
22	38.1	37.9	32.6	38.1	32.6
23	29.2	30.4	28.2	29.7	28.1
24	16.8	18.0	15.5	17.9	15.9
25	16.9	17.4	15.7	19.3	16.3
26	16.9	18.2	17.3	16.9	16.6
27	15.4	25.4	26.1	15.4	22.9
28	179.4	180.5	183.5	179.4	180.7
29	110.4	19.3	32.8	110.5	32.4
30	20.0	24.2	23.1	19.9	22.8

[a] Measured in pyridine-d_5[a] and chloroform-d[b] in 125 MHz and in methanol-d_4[c] in 100 MHz. δ_C in ppm.

Compound **3** was isolated as a white amorphous powder. The ^{1}H NMR spectrum (Table 1) displayed seven angular methyl signals at δ_H 1.13 (3H, s, H-27), 0.98 (3H, s, H-26), 0.92 (3H, s, H-30), 0.91 (3H, s, H-24), 0.90 (3H, s, H-29), and 0.77 (3H, s, H-25); an olefinic proton at δ_H 5.28 (1H, t, J = 3.5 Hz, H-12); and one oxygenated methine proton at δ_H 3.22 (1H, dd, J = 11.3, 4.4 Hz, H-3). The ^{13}C NMR spectrum (Table 2) exhibited 30 carbon signals, including seven methyl carbons, two olefinic carbons at δ_C 143.8 (C-13) and 122.7 (C-12), and a downfield carboxylic acid carbon at δ_C 183.5 (C-28). The NMR data suggested that compound **3** corresponded to an oleane-type triterpenoid, characterized by a C-28 carboxylic acid group and a 3-hydroxyl substituent. Based on these spectroscopic data and comparison with literature, compound **3** was identified, commonly known as oleanolic acid.[17]

Compound **4** was obtained as a white amorphous powder. The ^{1}H-NMR spectrum (Table 1) exhibited six methyl groups at δ_H 1.79 (3H, s, H-30), 1.28 (3H, s, H-24), 1.06 (9H, m, H-23, 25, 27), and 0.91 (3H, s, H-26); an olefinic proton at δ_H 4.95 (1H, s, H-29a) and 4.78 (1H, s, H-29b); as well as two oxygenated methine protons at δ_H 4.11 (1H, td, J = 10.3, 4.2 Hz, H-2) and 3.41 (1H, d, J = 9.2 Hz, H-3). The ^{13}C-NMR spectrum (Table 2) displayed 30 carbon signals, including six methyls, two oxygenated carbons at δ_C 84.3 (C-3) and 69.3 (C-2), two olefinic carbons at δ_C151.8 (C-20) and 110.5 (C-29), and one carboxylic acid carbon at δ_C 179.4 (C-28). The overall skeleton of compound **4** corresponded to a lupane-type triterpenoid closely related to betulinic acid and was similar to the structure of compound **2**. Based on these spectroscopic features and comparison with literature data, compound **4** was identified as 2-hydroxybetulinic acid, also known as alphitolic acid.[23]

Compound **5** was obtained as a white amorphous powder. The ^{1}H-NMR spectrum (Table 1) showed seven methyl groups at δ_H 1.13 (3H, s, H-27), 0.98 (3H, s, H-30), 0.97 (3H, s, H-25), 0.91 (3H, s, H-23), 0.87 (3H, s, H-24), 0.78 (3H, s, H-26), and 0.77 (3H, s, H-29); an olefinic proton at δ_H 5.22 (1H, t, J = 3.4 Hz, H-12); and two oxygenated methine protons at δ_H 3.58 (1H, ddd, J = 11.3, 9.6, 4.3 Hz, H-2β) and 2.87 (1H, d, J = 9.6 Hz, H-3α). The ^{13}C-NMR spectrum (Table 2) displayed 30 carbon signals, including seven methyls, two oxygenated carbons at δ_C 83.3 (C-3) and 68.3 (C-2), two olefinic carbons at δ_C 144.2 (C-13) and 122.2 (C-12), and one carboxylic acid carbon at δ_C 180.7 (C-28). The evidence indicated that compound **5** corresponded to an oleane-type triterpenoid, similar to oleanolic acid (**3**), except for bearing more 2-hydroxyl substituents at position C-2. Based on these spectroscopic data and comparison with literature, compound **5** was identified and is commonly known as maslinic acid.[24]

3-*O-cis-p*-Coumaroyl alphitolic acid (**6**): white amorphous powder: ^{1}H NMR (400 MHz, $CDCl_3$): δ_H 7.60 (1H, d, J = 8.5 Hz, H-2″, 6″), 6.89 (1H, d, J = 12.7 Hz, H-3′), 6.77 (1H, d, J = 8.7 Hz, H-3″, 5″), 5.89 (1H, d, J = 12.6 Hz, H-2′), 4.74 (1H, s, H-29a), 4.62 (1H, s, H-29b), 4.53 (1H, d, J = 10.0 Hz, H-3), 3.86 (1H, m, H-2), 1.70 (3H, s, H-30), 0.97 (3H, s, H-24), 0.92 (3H, s, H-27), 0.89 (3H, s, H-25). 0.88 (3H, s, H-23), and 0.79 (3H, s, H-26). ^{13}C NMR (100 MHz, $CDCl_3$): δ_C 181.4 (C-28), 168.1 (C-1′), 157.37 (C-4″), 150.4 (C-20), 144.7 (C-3′), 132.5 (C-2″, 6″), 127.3 (C-1″), 117.0 (C-3″), 116.1 (C-5″), 115.2 (C-2′) 110.0 (C-29), 85.0 (C-3), 68.2 (C-2), 56.5 (C-17), 55.5 (C-5), 50.5 (C-18), 49.4 (C-9), 48.0 (C-1), 47.1 (C-19), 42.6 (C-14), 40.9 (C-8), 39.6 (C-13), 38.6 (C-22), 38.5 (C-4), 37.2 (C-10), 34.3 (C-7), 32.3 (C-16), 30.73 (C-21), 29.8 (C-15), 28.6 (C-23), 25.5 (C-12), 21.1 (C-11), 19.5 (C-30), 18.4 (C-25), 17.6 (C-6), 17.5 (C-24), 16.2 (C-26), and 14.8 (C-27).

3-*O-trans-p*-Coumaroyl alphitolic acid (**7**): white amorphous powder: ^{1}H NMR (400 MHz, CD_3OD): δ_H 7.63 (1H, d, J = 15.9 Hz, H-3′), 7.47 (2H, d, J = 8.6 Hz, H-6″, H-2″), 6.81 (2H, d, J = 8.6 Hz, H-5″, H-3″), 6.39 (1H, d, J = 15.9 Hz, H-2′), 4.72 (1H, d, J = 1.5 Hz, H-29a), 4.61 (1H, H-29b), 4.63 (2H, d, J = 10.0 Hz, H-3), 3.83 (1H, td, J = 11.3, 4.6 Hz, H-2), 3.03 (1H, td, J = 10.4, 4.2 Hz, H-19), 1.71 (3H, s, H-30), 1.04 (3H, s, H-24), 1.00 (3H, s, H-27), 0.90 (3H, s, H-25), 0.93 (3H, s, H-23), and 0.88 (3H, s, H-26). ^{13}C NMR (100 MHz, CD_3OD): δ_C 178.8 (C-28), 167.4 (C-1′), 158.7 (C-4″), 150.7 (C-20), 143.5 (C-3′), 132.4 (C-2″, 6″), 126.6 (C-1″), 116.2 (C-3″, 5″), 114.5 (C-2′), 109.0 (C-29), 84.0 (C-3), 66.6 (C-2), 56.2 (C-17), 55.4 (C-5), 50.7 (C-18, 9), 49.2 (C-1), 47.3 (C-19), 42.5 (C-14), 40.8 (C-8), 39.3 (C-13), 38.4 (C-22), 38.3 (C-4), 36.9 (C-10), 34.2 (C-7), 32.1 (C-16), 30.5 (C-21), 29.6 (C-15), 27.9 (C-23), 25.6 (C-12), 21.0 (C-11), 18.4 (C-30), 18.2 (C-25), 16.8 (C-6), 16.7 (C-24), 15.4 (C-26), and 13.9 (C-27).

2-*O-trans-p*-Coumaroyl alphitolic acid (**8**): white amorphous powder: ^{1}H NMR (400 MHz, pyridine-d_5): δ_H 7.57 (2H, d, J =

Table 3 PTP1B and α-glucosidase inhibitory activity of the isolated compounds **1–15**

	IC_{50} (μM)	
Compound	PTP1B	
EtOH ex.	52% (100 μg mL^{-1})	
$CHCl_3$ Fr.	59% (100 μg mL^{-1})	α-glucosidase
1	17.02 ± 0.27	7.02 ± 0.31
2	8.75 ± 0.08	6.75 ± 0.16
3	11.06 ± 0.52	7.06 ± 0.23
4	90.90 ± 0.35	—
5	>100	—
6	>100	—
7	>100	—
8	>100	—
9	>100	—
10	60.92 ± 1.31	—
11	>100	—
12	>100	—
13	53.42 ± 0.12	—
14	>100	—
15	>100	—
Ursolic acid[a]	8.65 ± 0.75	
Acarbose		197.0 ± 3.8

[a] Positive control and "—" did not test.

8.5 Hz, H-6″, 2″), 7.17(2H, d, J = 8.5 Hz, H-5″, 3″), 8.05 (1H, d, J = 15.9 Hz, H-3′), 6.65(1H, d, J = 15.9 Hz, H-2′), 5.66 (1H, ddd, J = 4.4, 10.9, 10.9 Hz, H-2), 4.97 (1H, d, J = 2.18 Hz, H-29a), 4.82 (1H, s, H-29b), 3.67 (1H, d, J = 9.88 Hz, H-3), 1.82 (3H, s, H-30), 1.31 (3H, s, H-24), 1.12 (3H, s, H-27), 1.09 (3H, s, H-25), 1.04 (3H, s, H-23), and 1.02 (3H, s, H-26). ^{13}C NMR (100 MHz, pyridine-d_5): δ_C 179.2 (C-28), 167.8 (C-1′), 161.7 (C-4″), 151.7 (C-20), 145.0 (C-3′), 130.9 (C-3″, 5″), 126.5 (C-1″) 117.1 (C-2″, 6″), 116.3 (C-2′), 110.3 (C-29), 80.1 (C-3), 74.1 (C-2), 56.9 (C-17), 56.0 (C-5), 51.2 (C-9,18), 50.1 (C-1), 48.1 (C-19), 45.3 (C-14), 43.2 (C-14), 41.4 (C-8), 40.8 (C-13), 39.1 (C-22), 38.9 (C-4), 37.9 (C-10), 34.9 (C-7), 33.2 (C-16), 31.4 (C-21), 30.5 (C-15), 29.4 (C-23), 26.3 (C-12), 21.6 (C-11), 19.7 (C-30), 19.1 (C-25), 17.7 (C-6), 17.7 (C-24), 16.6 (C-26), and 15.2 (C-27).

2-*O*-*cis*-*p*-Coumaroyl alphitolic acid (**9**): white amorphous powder: ^{1}H NMR (400 MHz, $CDCl_3$): δ_H 7.60 (2H, dd, J = 8.4, 1.3 Hz, H-2″, 6″), 6.83 (1H, d, J = 12.7 Hz, H-3′), 6.78 (2H, dd, J = 8.5, 1.6 Hz, H-3″, 5″), 5.79 (1H, dd, J = 12.7, 1.7 Hz, H-2′), 4.97(1H, ddd, J = 10.4, 10.4, 4.8 Hz, H-2), 4.70 (1H, s, H-29a), 4.57 (1H, s, H-29b), 3.16 (1H, d, J = 10.4 Hz, H-3), 2.96 (1H, ddd, J = 4.0, 10.0, 10.0 Hz, H-19), 1.65 (3H, s, H-30), 1.01 (3H, s, H-24), 0.95 (3H, s, H-27), 0.93 (3H, s, H-25), 0.91 (3H, s, H-23), and 0.82 (3H, s, H-26). ^{13}C NMR (100 MHz, $CDCl_3$): δ_C 179.1 (C-28), 166.8 (C-1′), 156.5 (C-4″), 150.2 (C-20), 143.6 (C-3′), 132.2 (C-2″, 6″), 117.3 (C-3″, 5″), 114.9 (C-2′), 109.7 (C-29), 80.7 (C-3), 73.4 (C-2), 56.1 (C-17), 55.2 (C-5), 50.4 (C-18), 49.2 (C-9), 46.8 (C-1), 43.9 (C-19), 42.4 (C-14), 40.7 (C-8), 39.7 (C-13), 38.5 (C-22), 38.2 (C-4), 36.9 (C-10), 34.1 (C-7), 32.1 (C-16), 30.4 (C-21), 29.6 (C-15), 28.3 (C-23), 25.3 (C-12), 20.9 (C-11), 19.3 (C-30), 18.1 (C-25), 17.1 (C-6), 16.4 (C-24), 15.9 (C-26), and 14.6 (C-27).

Ceanothic acid (**10**): white amorphous powder: ^{1}H NMR (400 MHz, $CDCl_3$ + CD_3OD 10:1): δ_H 4.61 (1H, d, J = 0.9 Hz, H-29a), 4.47 (1H, d, J = 0.7 Hz, H-29b), 4.04 (1H, s, H-3), 2.90 (2H, td, J = 10.4, 4.3 Hz, H-1), 2.42 (1H, s, H-2), 2.15 (2H, dd, J = 12.7, 2.6 Hz H-5), 1.57 (3H, s, H-30), 1.01 (3H, s, H-23), 0.98 (3H, s, H-25), 0.87 (3H, s, H-24), 0.86 (3H, s, H-26), and 0.83 (3H, s, H-27). ^{13}C-NMR (100 MHz, $CDCl_3$ + CD_3OD 10:1): δ_C 179.25 (C-28), 177.9 (C-1), 150.6 (C-20), 109.4 (C-29), 84.8 (C-3), 65.9 (C-2), 56.6 (C-5), 56.2 (C-17), 50.0 (C-18), 49.3 (C-10), 49.2 (C-19), 44.4 (C-9), 43.2 (C-4), 43.0 (C-14), 41.6 (C-8), 38.7 (C-13), 37.2 (C-22), 34.0 (C-7), 32.4 (C-16), 30.81 (C-21), 30.65 (C-15), 29.89, 25.44 (C-12), 23.56 (C-11), 19.26 (C-24), 19.03 (C-30), 18.75 (C-6), 18.54 (C-25), 16.39 (C-26), and 14.65 (C-27).

Zizyberanalic acid (**11**): white amorphous powder: ^{1}H NMR (400 MHz, pyridine-d_5): δ_H 10.16 (1H, d, J = 4.7 Hz, CHO-2), 4.93 (1H, d, J = 2.0 Hz, H-29), 4.77 (1H, d, J = 2.2 Hz, H-29), 4.71 (1H, d, J = 8.8 Hz, H-3β), 3.50 (1H, td, J = 11.5, 5.3 Hz, H-19), 1.77 (3H, s, H-30) 1.25 (3H, s, H-23), 1.04 (3H, s, H-25), 1.04 (3H, s, H-24), 1.01(3H, s, H-26), and 1.01 (3H, s, H-27). ^{13}C NMR (100 MHz, pyridine-d_5): δ_C 206.7 (C-1), 179.3 (C-28), 151.6 (C-20), 110.5 (C-29), 81.2 (C-2), 74.3 (C-3), 63.4 (C-5), 56.9 (C-17), 50.8 (C-18), 50.1 (C-9), 48.7 (C-4), 48.3 (C-19), 43.5 (C-8), 42.7 (C-14), 41.7 (C-10), 38.9 (C-13), 38.0 (C-22), 35.0 (C-7), 33.3 (C-16), 31.6 (C-15), 30.8 (C-21), 26.8 (C-23), 26.1 (C-25), 26.0 (C-12), 25.3 (C-11), 19.9 (C-30), 18.9 (C-6), 17.5 (C-24), 15.5 (C-26), and 15.3 (C-27).

trans-*p*-Coumaroyl betulinic acid (**12**): ^{1}H NMR (500 MHz, chloroform-*d*): δ_H 7.64 (1H, d, J = 15.9 Hz, H-3′), 7.41 (2H, d, J = 8.6 Hz, H-2″, 6″), 6.83 (2H, d, J = 8.6 Hz, 3″, 5″), 6.33 (1H, d, J = 15.9 Hz, H-2′), 5.34 (1H, m, H-3), 4.74 (1H, s, H-29a), 4.62 (1H, s, H-29b), 1.69 (3H, s, H-30), 0.98 (3H, s, H-27), 0.94 (3H, s, H-26), 0.93 (3H, s, H-24), 0.92 (3H, s, H-23), and 0.91 (3H, s, H-25).

Betulonic acid (**13**): ^{1}H NMR (400 MHz, chloroform-*d*): δ_H 4.62 (1H, s, H-29), 4.49 (1H, s, H-29), 1.58 (3H, s, H-30), 0.96 (3H, s, H-23), 0.91 (3H, s, H-27), 0.88 (3H, s, H-26), 0.87 (3H, s, H-24), and 0.81 (3H, s, H-25). ^{13}C NMR (100 MHz, chloroform-*d*): δ_C 219.9 (C-3), 179.3 (C-28), 150.6 (C-20), 109.5 (C-29), 56.2 (C-17), 54.8 (C-5), 49.8 (C-9), 49.1 (C-19), 47.4 (C-18), 46.9 (C-4), 42.4 (C-14), 40.6 (C-8), 39.6 (C-1), 38.3 (C-13), 37.1 (C-10), 36.8 (C-22), 34.1 (C-7), 33.5 (C-16), 32.2 (C-15), 30.5 (C-21), 29.6 (C-23), 26.6 (C-2), 25.5 (C-12), 21.4 (C-11), 20.9 (C-6), 19.6 (C-26), 19.2 (C-30), 15.9 (C-25), 15.6 (C-24), and 14.5 (C-27).

Ursolic acid (**14**): white amorphous powder: ^{1}H NMR (500 MHz, pyridine-d_5): δ_H 5.52 (1H, t, J = 3.3 Hz, H-12), 3.49 (1H, dd, J = 10.2, 5.9 Hz, H-3α), 2.67 (1H, d, J = 11.3 Hz, H-18), 1.27 (3H, s, H-23), 1.25 (3H, s, H-27),1.09 (3H, s, H-26), 1.05 (3H, s, H-24), 1.05 (3H, s, H-30), 0.99 (3H, d, J = 6.3 Hz, H-29), and 0.93 (3H, s, H-25). ^{13}C NMR (125 MHz, pyridine-d_5): δ_C 180.4 (C-28), 139.8 (C-13), 126.2 (C-12), 78.7 (C-3), 56.4 (C-18), 54.1 (C-5), 48.6 (C-17), 43.0 (C-9), 40.5 (C-14), 40.0 (C-4), 39.9 (C-8), 39.9 (C-1), 39.6 (C-22), 37.9 (C-10), 37.8 (C-7), 34.1 (C-19), 31.6 (C-20), 30.5 (C-15), 29.3 (C-21), 29.2 (C-27), 28.6 (C-11), 25.4 (C-2), 24.4 (C-30), 24.1 (C-23), 21.9 (C-16), 19.3 (C-29), 18.0 (C-6), 17.9 (C-25), 17.0 (C-24), and 16.2 (C-26).

Oleanonic acid (**15**): ^{1}H NMR (400 MHz, chloroform-*d*): δ_H 5.30 (t, J = 3.7 Hz, 1H, H-12), 2.83 (dd, J = 13.9, 4.4 Hz, 1H, H-2), 1.14 (3H, s, H-27), 1.08 (3H, s, H-23), 1.04 (3H, s, H-24), 1.03

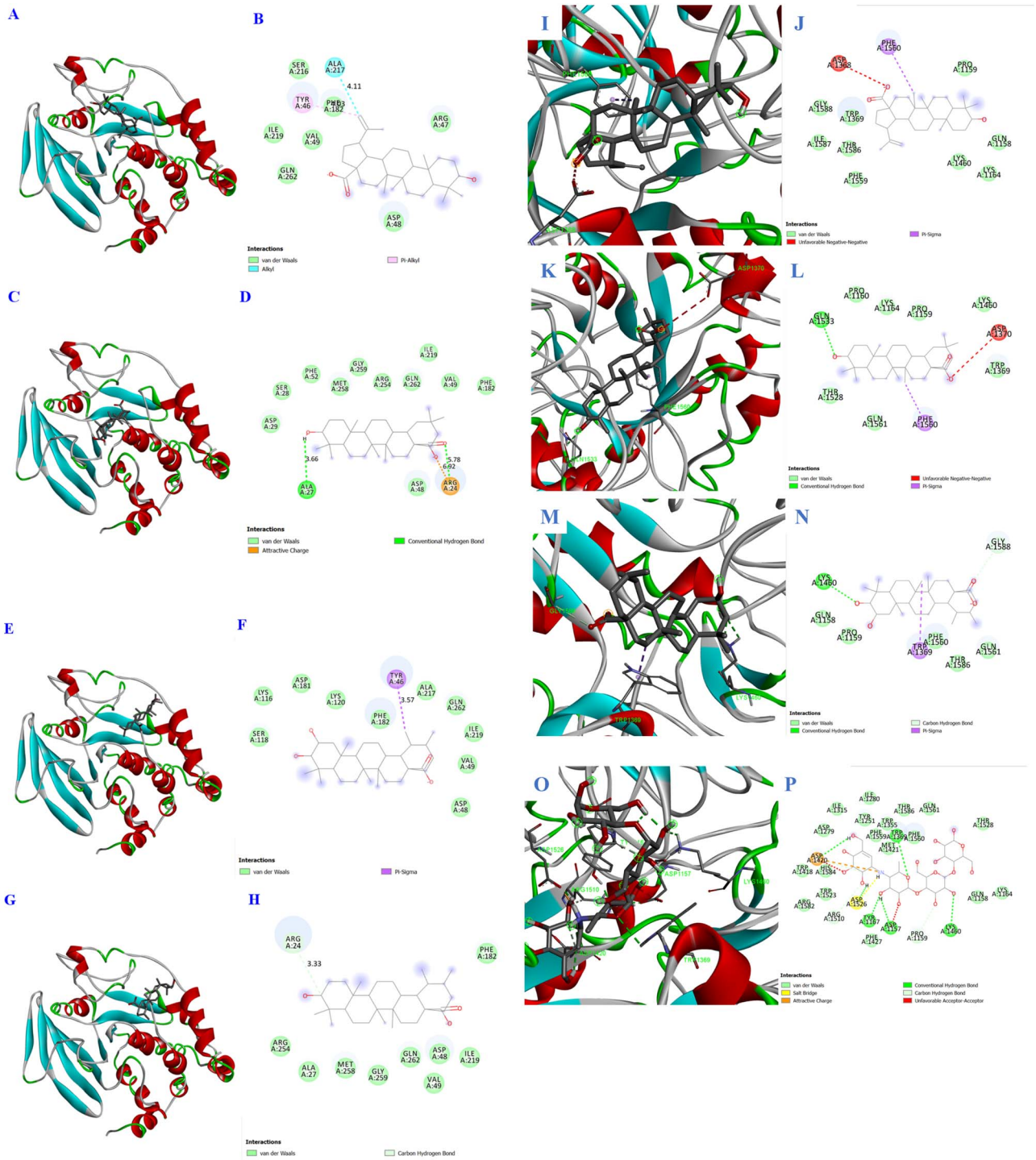

Fig. 3 3D docking poses and 2D interaction diagrams of PTP1B inhibition with the compounds **1–3** ((**1**: A and B), (**2**: C and D), (**3**: E and F), and (ursolic acid: G and H)) and α-glucosidase with the compounds **1–3** ((**1**: I and J), (**2**: K and L), (**3**: M and N), and (acarbose: O and P)).

(3H, s, H-25), 0.93 (3H, s, H-26), 0.90 (3H, s, H-29), and 0.81 (3H, s, H-30). ^{13}C NMR (100 MHz, chloroform-*d*): δ_C 218.2 (C-3), 183.9 (C-28), 143.7 (C-13), 122.6 (C-12), 55.4 (C-5), 47.6 (C-9), 47.0 (C-4), 46.7 (C-17), 45.9 (C-19), 41.9 (C-14), 41.2 (C-18), 39.4 (C-8), 39.2 (C-1), 36.9 (C-10), 34.3 (C-21), 33.9 (C-22), 33.2 (C-7), 32.5 (C-29), 32.3 (C-2), 30.8 (C-20), 29.9 (C-15), 27.8 (C-23), 26.6 (C-29), 26.0 (C-27), 23.7 (C-26), 23.6 (C-30), 23.1 (C-16), 21.6 (C-), 19.7 (C-6), 17.1 (C-25), and 15.2 (C-24).

In vitro PTP1B screening

Protein tyrosine phosphatase 1B (PTP1B) is known to catalyze the dephosphorylation of the insulin receptor kinase, thereby

Table 4 Molecular docking interactions of the active compounds **1–3** and the targeted proteins

Compound	Binding energy (kcal mol^{-1})	Interaction
1	−7.4	• Alkyl: Ala217 • π-Alkyl: Tyr46 • vdW: Ser216, Phe182, Val49, Ile219, Gln262, Asp48, Arg47
2	−6.6	• π-Sigma: Tyr46 • vdW: Ser118, Lys116, Asp181, Lys120, Phe158, Ala217, Gln262, Ile219, Val49, Asp48
3	−7.4	• H-bond: Ala27 • vdW: Asp29, Ser28, Phe52, Met258, Gly259, Arg254, Gln262, Ile219, Val49, Phe182, Asp48
Ursolic acid	−6.6	• H-bond: Arg24 • vdW: Arg254, Ala27, Met258, Gly259, Gln262, Asp48, Val49, Ile219, Phe182
1	−7.5	• π–σ: Phe1560 • Unfavorable negative–negative: Asp1368 • vdW: Gly1588, Trp1369, Ile1587, Thr1586, Phe1559, Gln1158, Lys1460, Lys1164, Pro1159
2	−8.2	• H-bond: Gln1533 • π–σ: Phe1560 • Unfavorable negative–negative: Asp1370 • vdW: Pro1160, Lys1164, Pro1159, Lys1460, Thr1528, Gln1561, Trp1369
3	−8.1	• H-bond: Lys1460 • Carbon H-bond: Gly1588 • π–σ: Trp1369 • vdW: Gln1158, Pro1159, Thr1586, Gln1561, Phe1560
Acarbose	−9.8	• H-bond: Asp1157, Asp1420, Tyr1167, Asp1526, Lys1460, Trp1369 • Salt bridge: Asp1526 • Attractive charge: Asp1420 • Carbon H-bond: Pro1159, Arg1510 • Unfavorable acceptor–acceptor: Asp1157 • vdW: Trp1418, His 1584, Trp1523, Arg1582, Phe1427, Gln1158, Lys1164, Thr1528, Gln1561, Phe1560, Thr1586, Met1421, Phe1559, Tyr1251, Ile1280, Ile1315, Asp1279

attenuating insulin signal transduction, which contributes to impaired glucose homeostasis and increased body weight. Consequently, PTP1B inhibitors are considered potential therapeutic agents for diabetes, as they enhance insulin sensitivity by improving signaling pathways. This study assessed isolates **1–15** for their inhibitory activity against PTP1B. The results demonstrated that some compounds (**1–4**, **10**, **13**) showed significant dose-dependent inhibition, with IC_{50} values ranging from 8.75–90.90 μM. Among them, compound **2** showed the potential inhibition of PTP1B enzyme activity, with an IC_{50} value of 8.75 μM, comparable to the positive control, ursolic acid (8.65 μM). Compounds **3** and **1** showed strong PTP1B inhibition, with IC_{50} values of 11.06 and 17.02 μM, respectively. Compounds **10** and **15** showed moderate activity, with IC_{50} values of 53.42 and 60.92 μM, respectively, while compound **4** exhibited a weak inhibitory effect, with an IC_{50} value of 90.90 μM; in contrast, compounds **5** and others did not show this inhibition in the same model (see Table 3).

In vitro α-glucosidase screening

Considering the potent PTP1B inhibitory activities of compounds **1–3**, their effects on α-glucosidase were subsequently investigated to further evaluate their antidiabetic potential through complementary mechanisms. As presented in Table 3, compounds **1–3** exhibited strong α-glucosidase inhibitory activity, with IC_{50} values of 7.02 ± 0.31, 6.75 ± 0.16, and 7.06 ± 0.23 μM, respectively. These results indicated that those compounds possessed comparable inhibitory potency, with compound **2** showing slightly stronger activity among them. Although acarbose, a standard α-glucosidase inhibitor, was included for direct comparison, the observed IC_{50} values in the low micromolar range suggested pharmacologically relevant activity. In contrast, compounds **4–15** were not evaluated in this assay due to their weak or negligible activities observed during the initial screening process. The consistent inhibitory effects of compounds **1–3** against α-glucosidase highlighted their potential as target agents for the regulation of glucose homeostasis, supporting their further investigation as promising candidates for antidiabetic drug development.

Molecular docking

Molecular docking (Fig. 3 and Table 4) was conducted to elucidate the binding modes and affinities of compounds **1–3** toward PTP1B and α-glucosidase. For PTP1B, all compounds exhibited comparable binding energies ranging from −6.6 to −7.4 kcal mol^{-1}, indicating favorable interactions within the catalytic pocket. Compounds **1** and **3** showed slightly stronger affinities, which may be attributed to their ability to establish stable contacts with key residues, such as Tyr46, Val49, Ala217, and Gln262. In particular, compound **3** formed an additional hydrogen bond within the active site, providing further stabilization compared to compound **1**, which primarily relied on hydrophobic and van der Waals interactions.

For α-glucosidase, compounds **1–3** demonstrated moderate binding affinities (−7.5 to −8.2 kcal mol^{-1}), with compound **2** exhibiting the most favorable binding energy. This enhanced affinity was consistent with its ability to form a hydrogen bond with Gln1533, along with π–σ interaction with Phe1560 and multiple van der Waals contacts involving residues, such as Trp1369 and Lys1460. Similarly, compound **3** formed a hydrogen bond with Lys1460 and a carbon–hydrogen bond with Gly1588, contributing to stabilization within the binding pocket. In contrast, compound **1** lacked classical hydrogen bonding but maintained binding through π–σ interaction with Phe1560 and extensive van der Waals interactions.

Although all compounds displayed lower binding affinities than acarbose (−9.8 kcal mol^{-1}), which formed multiple hydrogen bonds with catalytic residues (*e.g.*, Asp1157, Asp1420, Asp1526, and Lys1460), the observed interactions suggested that compounds **1–3** could effectively occupy the active site. Notably, the presence of hydroxyl groups, particularly in

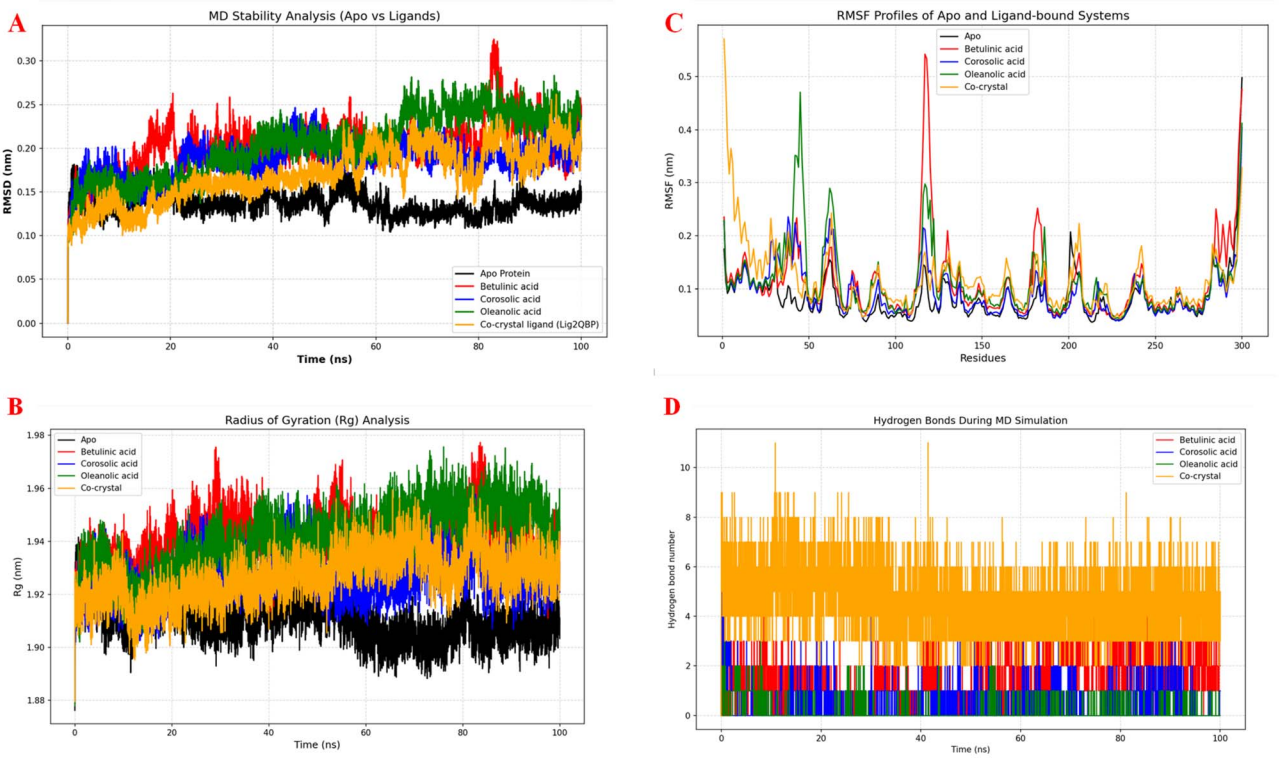

Fig. 4 MD simulations of the RMSD profiles (A), radius of gyration plots (B), RMSF profiles (C), and the number of hydrogen bonds during the MD run (D).

compound **2**, appeared to facilitate additional polar interactions, thereby enhancing binding affinity. Overall, these results supported the potential of the tested compounds as moderate α-glucosidase inhibitors through a combination of hydrophobic and hydrogen bonding interactions.

All three compounds were pentacyclic triterpenoids bearing a carboxylic moiety (–COOH) at C-28; however, the number and position of hydroxyl groups, as well as the structural scaffold, played a crucial role in determining their inhibitory potency. Specifically, corosolic acid (**2**, ursane-type triterpenoid) contained a hydroxyl group at C-2, in addition to the hydroxyl group at C-3, which most likely enhances inhibitory effects against PTP1B and α-glucosidase *in vitro*, while also improving hydrogen bonding interactions and binding affinity *in silico*. This observation was consistent with docking results, where compound **2** formed additional hydrogen bonding interactions, contributing to enhanced binding affinity. The slightly lower activity of oleanolic acid (**3**) compared with that of corosolic acid (**2**) may be attributed to the absence of the additional hydroxyl group at C-2, rather than differences in the methyl substitution pattern. Similarly, the relatively low activity of betulinic acid (**1**) may be attributed to its limited number of hydroxyl groups, which reduced its capacity to form stabilizing hydrogen bond interactions within the enzyme active site. Comparison between structurally related pairs (**1** *vs.* **4** and **3** *vs.* **5**) further supported the importance of hydroxyl substitution at C-2 in modulating inhibitory activity. It indicated that the hydroxy group located at C-2 of pentacyclic triterpenoids may decrease the inhibitory potency against PTP1B and α-glucosidase. In contrast, the enhanced activity of compound **2** suggested that the additional hydroxyl group at C-2 played a crucial role in improving the binding affinity and inhibitory potency.

Table 5 Binding free energy over 100 ns simulations (kcal mol^{-1}) of the active compounds **1–3**

Compound	Δ*G*_bind (kcal mol^{-1})
Lig2QBP (co-crystal)	−42.15
Betulinic acid (**1**)	−19.30
Corosolic acid (**2**)	−14.44
Oleanolic acid (**3**)	−13.93

Molecular dynamics

Molecular dynamics simulations (Fig. 4 and Table 5) were performed over 100 ns to evaluate the stability and dynamic behavior of PTP1B–ligand complexes. All systems reached equilibrium after the initial simulation phase and remained stable throughout the trajectory, as indicated by relatively constant RMSD values. The apo protein exhibited minimal fluctuations, whereas ligand-bound systems showed slightly higher RMSD values, reflecting conformational adjustments upon ligand binding. Among the tested compounds, the complex with compound **2** displayed the most stable trajectory,

Table 6 *In silico* ADME profiles of the active compounds **1–3**

Compound	**1**	**2**	**3**
Molecular weight	456.70	472.70	456.70
No. of H-bond acceptor	3.0	4.0	3.0
No. of H-bond donor	2.0	3.0	2.0
No. of rotatable bonds	2.0	1.0	1.0
TPSA (Å^2)	57.53	77.76	57.53
log *P*	3.796	3.613	3.983
log *S*	−4.848	−4.5	−4.988
Gastrointestinal absorption	Low	High	Low
log K_p (skin permeation, cm s^{-1})	−3.26	−4.66	−3.77
CYP1A2 inhibitor	No	No	No
CYP2C19 inhibitor	No	No	No
CYP2C9 inhibitor	Yes	No	No
CYP2D6 inhibitor	No	No	No
CYP3A4 inhibitor	No	No	No
Lipinski violation(s)	Yes, 1 violation	Yes, 1 violation	Yes, 1 violation

while compounds **1** and **3** showed moderate but acceptable fluctuations.

The radius of gyration (R_g) values remained consistent across all systems, suggesting that ligand binding did not significantly alter the overall compactness of the protein structure. Residue-level flexibility analysis (RMSF) revealed localized fluctuations in loop regions, while key active-site residues remained relatively stable, indicating that ligand binding did not disrupt the structural integrity of the catalytic site. Notably, the complex with compound **2** exhibited relatively low residue fluctuations around the binding pocket, further supporting its enhanced stability.

Hydrogen bond analysis demonstrated that the reference ligand maintained a more persistent hydrogen bonding network throughout the simulation, whereas compounds **1–3** formed fewer and more transient hydrogen bonds. Nevertheless, compounds **2** and **3** consistently maintained at least one hydrogen bond during the simulation, contributing to their stable binding. In contrast, compound **1** showed relatively few hydrogen bonding interactions, which may explain its relatively low binding stability.

Table 7 *In silico* toxicity profiles of the active compounds **1–3**

Compound	**1**	**2**	**3**
Acute LD_{50} (mg kg^{-1})	2610	2000	2000
Carcinogenesis	**Yes**	**Yes**	**Yes**
Liver injury I (DILI)	No	No	**Yes**
Liver injury II	No	No	No
Micronucleus	No	No	No
hERG blockers	No	No	No
Androgen receptor	No	No	No
Androgen receptor-LBD	No	No	No
Estrogen receptor	No	No	No
Estrogen receptor-LBD	No	No	No
GABA receptor (GABAR)	**Yes**	No	**Yes**
Thyroid receptor	No	No	No

Binding free energy calculations (MM/GBSA) further supported these observations, with all compounds exhibiting favorable binding energies. Among them, compound **1** showed slightly more favorable binding energy, despite forming fewer hydrogen bonds, suggesting that hydrophobic interactions played a significant role in stabilizing the complex. Overall, the MD results confirmed that the ligand–protein complexes were dynamically stable and highlighted the combined contribution of hydrogen bonding and hydrophobic interactions in maintaining binding within the active site.

In silico ADME and toxicity profiles prediction

The *in silico* ADMET predictions of compounds **1–3**, obtained using the ADMETlab 3.0 web tool, are summarized in Table 6. All three compounds complied with Lipinski's Rule of Five, indicating a high likelihood of oral bioavailability. In addition, gastrointestinal absorption was predicted to be high for **2** but low for **1** and **3**, further supporting their favorable bioavailability. The cytochrome P450 (CYP) enzyme family, including CYP1A2, CYP2C19, CYP2C9, CYP2D6, CYP3A4, and CYP2B6, originating primarily from the liver and intestines, plays a key role in drug metabolism through oxidative processes. Notably, compound **1** exhibited a potential inhibition of CYP2C9, whereas compounds **2** and **3** did not show activation for CYP2C9, and all three compounds also did not activate others (CYP1A2, CYP2C19, CYP2D6, and CYP3A4 inhibitors). From the above data, although **1–3** cannot be considered further clinically or for pharmacokinetic interactions when co-administered with other drugs, as mechanism-based inhibitors of the cytochrome P450 (CYP) enzyme family, they can play an essential role in elucidating the direction of the *in vivo* pharmacokinetic profile and interaction risks.

The toxicity profiles of the three compounds were further predicted using a computational tool, Deep-PK. All three compounds exhibited relatively low acute toxicity, with LD_{50} values of 2610, 2000, and 2000 mg kg^{-1}, respectively (Table 7), which were higher than the reference value of 1000 mg kg^{-1}, cautioning their potential applications. In addition, the prediction results indicated the possible effects of compounds **1–3** on carcinogenesis, drug-induced liver injury (DILI), and the GABA receptor (GABAR). Interactions that trigger carcinogenesis may contribute to the accumulation of genetic alterations, affecting cellular identity and proliferation and ultimately leading to cancer.[25] Association with DILI could result in various forms of liver trauma, ranging from mild lacerations to severe damage,[26] while binding to GABAR may significantly impact normal brain function.[27] Furthermore, none of the compounds showed predicted interactions with key receptors, including micronucleus, hERG blockers, androgen and androgen receptor-LBD, estrogen and estrogen receptor-LBD, and thyroid receptor, suggesting a relatively low risk of hormonal imbalance or cardiac arrhythmias. Overall, these *in silico* predictions suggest that although compounds **1–3** may hold promise for further development, their potential risks warrant careful consideration and additional investigation.

Conclusions

In conclusion, this study provided the first comprehensive investigation of pentacyclic triterpenoids from Vietnamese *Z. jujuba* Lamk. (Táo ta) fruits, integrating bioactivity-guided isolation with *in vitro* and *in silico* evaluations. Fifteen triterpenoids were successfully isolated and structurally characterized, among which betulinic acid (**1**), corosolic acid (**2**), and oleanolic acid (**3**) exhibited potent dual inhibitory activities against PTP1B and α-glucosidase, with IC_{50} values in the low micromolar range. This dual-target profile highlighted their potential relevance in regulating glucose homeostasis through complementary mechanisms. Molecular docking and molecular dynamics simulations further confirmed that these compounds could stably interact with key residues within the active sites of both enzymes, predominantly through hydrophobic contacts, van der Waals interactions, and limited hydrogen bonding. Structure–activity relationship analysis emphasized the importance of the C-28 carboxylic acid and C-3 hydroxyl groups for enzyme inhibition, while the presence and position of additional hydroxyl substituents and the triterpenoid scaffold (lupane, ursane, or oleanane type) significantly influenced binding affinity and biological activity. Moreover, *in silico* ADME and toxicity predictions indicated favorable drug-likeness, acceptable pharmacokinetic properties, and relatively low acute toxicity, supporting the suitability of these compounds as lead candidates. Although their binding affinities and interaction networks were less extensive than those of standard inhibitors, the observed biological activities and stable binding behaviors suggest that these natural triterpenoids represent promising scaffolds for further structural optimization. Overall, the findings of this study provide a scientific basis for the development of Vietnamese *Z. jujuba*-derived pentacyclic triterpenoids as a valuable natural source of antidiabetic agents, warranting further *in vivo* studies and mechanistic investigations to validate their therapeutic potential.

Overall, the integration of phytochemical, biochemical, and computational evidence underscored the scientific and pharmacological significance of *Z. jujuba* as a valuable natural resource for diabetes drug discovery. Future studies, including *in vivo* validation and mechanistic investigations, are warranted to establish the therapeutic potential and safety of these triterpenoids and advance them toward clinical application as natural antidiabetic agents.

Experimental

General experimental procedures

Chemical structures were drawn using ChemDraw 21.0, PerkinElmer. NMR spectra were recorded on a Bruker 400 MHz spectrometer, using tetramethylsilane (TMS) as the internal standard, and chemical shifts were expressed in δ values (ppm). Open-column chromatographic separations were carried out on silica gel NP (Merck, 63–200 μm), RP-18 silica gel (Merck, 75 μm), and Sephadex LH-20. Thin-layer chromatography (TLC) was performed on Merck silica gel 60 F_{254} plates. Preparative HPLC was conducted on a Hitachi system equipped with a UV detector (model 2996) using a YMC-Triart C18 column (4.6 × 250 mm, 5 μm; YMC Co., Ltd, Japan). The detection of compounds was achieved by spraying plates with 10% aqueous H_2SO_4, followed by heating for 3–5 min.

Plant material

The fruit of *Ziziphus jujuba* Lamk. (Táo Ta, Rhamnaceae) collected in October 2024 at Cao Lanh city, Dong Thap province, Vietnam. Dr Huynh Nguyen Khanh Tran performed the botanical identification by comparison with the depiction of Prof. Do Tat Loi[28] (pages 788–790), and the voucher specimen with registry no. MNP0010 was deposited at the Department of Organic and Medicinal Chemistry, Faculty of Pharmacy, University of Health Sciences, Vietnam National University Ho Chi Minh City (UHS-VNU).

Extraction and isolation

In the present study, the fresh fruits of *Ziziphus jujuba* Lamk. were air-dried under ambient conditions until reaching a stable weight prior to extraction, followed by grinding into a coarse powder to improve extraction efficiency and solvent penetration. A total of 6.5 kg of powdered *Z. jujuba* fruits was extracted three times with ethanol (20 L each) under reflux at temperatures of approximately 45–50 °C for 3 h per extraction. The combined extracts were concentrated under reduced pressure, and the residue was suspended in water and successively partitioned with *n*-hexane, chloroform, ethyl acetate, *n*-butanol, and water. Among these, the $CHCl_3$-soluble fraction (15.5 g) was subjected to silica gel column chromatography (80 × 12 cm, 63–200 μm, Merck) using a gradient of hexane–ethyl acetate (20 : 1 → 0 : 1, 2 L each) to yield ten fractions (Fr. CH1–CH10) based on TLC analysis. Fraction CH4 (3.3 g) was further separated by normal-phase silica gel column chromatography (60 × 6.5 cm), eluted with hexane–ethyl acetate (20 : 1, 2 L each), to afford eight fractions (Fr. CH4.1–CH4.8). Fraction CH4.6 (450 mg) was then purified by reversed-phase chromatography on an YMC RP-18 column (4.6 × 250 mm, 5 μm), eluted with MeOH–H_2O (from 4 : 1 to 1 : 0, 0.4 L each), to produce eight subfractions (Fr. CH4.6.1–CH4.6.8). Subfraction CH4.6.4 (245.0 mg) was further fractionated on a Sephadex LH-20 column using MeOH–H_2O (6 : 1, 0.4 L each), yielding eleven subfractions. Fr. CH4.6.4.7 (88.2 mg) was subsequently purified by HPLC (Hitachi system) with a gradient of 65–98% MeOH in H_2O containing 0.1% formic acid (flow rate: 1.0 mL min^{-1}, 60 min, PDA detection), affording compounds **1** (15.5 mg), **2** (11.9 mg), **6** (5.1 mg) and **7** (4.3 mg). Likewise, the purification of Fr. CH4.6.4.8 (100.3 mg) under similar conditions resulted in the isolation of six additional compounds: **3** (11.4 mg), **4** (13.6 mg), **5** (15.1 mg), **8** (3.9 mg), **9** (6.5 mg), and **10** (5.4 mg). The further purification of fraction CH4.7 (126.1 mg) by preparative HPLC, with a gradient of 65–98% MeOH in H_2O containing 0.1% formic acid (flow rate 1.0 mL min^{-1}, 60 min, PDA detection), yielded compounds **11** (8.4 mg), **12** (6.4 mg), **13** (3.6 mg), **14** (3.1 mg), and **15** (4.2 mg).

PTP1B inhibitory assay

The assay was lightly modified to suit our experimental conditions. Protein tyrosine phosphatase 1B (human

recombinant) was purchased from Biomol International LP, Plymouth Meeting, PA, and the inhibitory activities of the tested samples were evaluated using *p*-nitrophenyl phosphate (*p*-NPP) as a substrate.[29] Briefly, to each well (final volume 110 μL), 2 mM *p*-NPP and PTP1B in a buffer containing 50 mM citrate (pH 6.0), 0.1 M NaCl, 1 mM EDTA, and 1 mM dithiothreitol (DTT), were added with or without the sample. The plate was preincubated at 37 °C for 10 min, and then, 50 mL of *p*-NPP in buffer was added. Following incubation at 20 °C for 20 min, the reaction was terminated by adding 1 M NaOH. The amount of *p*-nitrophenyl produced after enzymatic dephosphorylation was estimated by measuring the absorbance at 405 nm using a VERSA Max microplate reader (Molecular Devices, Sunnyvale, CA). The non-enzymatic hydrolysis of 2 mM *p*-NPP was corrected by measuring the increase in absorbance at 405 nm, obtained in the absence of PTP1B enzyme. The inhibition (%) was calculated as follows: $(A_c - A_s)/A_c \times 100\%$, where A_c is the absorbance of the control, and A_s is the absorbance of the sample.[30]

α-Glucosidase inhibitory assay

The α-glucosidase inhibitory activity was evaluated using a slightly modified method described by Kurihara *et al.*[31] The reaction mixture consisted of 50 μL of 1.5 mM *p*-nitrophenyl-α-D-glucopyranoside, 50 μL of α-glucosidase (0.1 U mL^{-1}) prepared in 0.01 M phosphate buffer (pH 7.0), and 625 μL of the test sample at various concentrations (5, 10, 25, and 50 μM for compounds **1–3**). The mixture was incubated at 37 °C for 30 min, after which the reaction was terminated by the addition of 0.1 M Na_2CO_3. The absorbance of the reaction mixture was measured at 401 nm. The IC_{50} value was defined as the concentration of inhibitor required to suppress 50% of enzyme activity. Acarbose was used as the positive control, and all experiments were conducted in triplicate. The percentage of α-glucosidase inhibition was calculated using the following equation: α-glucosidase inhibition (%) = $(A_c - A_t)/A_c \times 100$, where A_c represents the absorbance of the control (enzyme without sample), and A_t represents the absorbance in the presence of the test sample. Data analysis was performed using the GraphPad Prism 8 software.[32]

Statistical analysis

Data were represented as the means ± standard deviations of three replicates. The Student's *t*-test was used for the statistical analysis of the noted differences. $P < 0.01$ was accepted as statistically significant.

Molecular docking simulation

The crystal structure of the PTP1B inhibitor complex with PDB ID 8SKL was obtained from the RCSB Protein Data Bank (https://www.rcsb.org). The co-crystallized ligand in the 8SKL complex was 5-[1-fluoro-3-hydroxy-7-(3-hydroxy-3-methylbutoxy)naphthalen-2-yl]-1,2,5-thiadiazolidine-1,1,3-trione.[33] As the crystallographic structure of *Saccharomyces cerevisiae* α-glucosidase was unavailable, the 3D structure, designated AF-P38158-F1 (MAL32), was retrieved from the AlphaFold Protein Structure Database (https://alphafold.ebi.ac.uk/entry/P38158). After downloading from the RCSB database, the co-crystallized ligand and water molecules were removed using UCSF Chimera version 1.18. The 3D structures of the ligands were retrieved from the PubChem database (https://pubchem.ncbi.nlm.nih.gov/). These structures were then assigned force fields and energy-minimized using the Gasteiger method *via* Antechamber. Docking preparation was performed, which included solvent removal, the addition of hydrogen atoms, and the assignment of atomic charges. AMBER ff14SB was applied to standard residues for charge assignment, and Gasteiger charges were calculated for the ligands using ANTECHAMBER, implemented in UCSF Chimera 1.18. The prepared protein and ligand structures were converted to the PDBQT format for docking using AutoDock Vina version 1.2. Grid Box parameters: center $x = -30.64$, center $y = 27.38$, center $z = -1.85$, size $x = 40$, size $y = 40$, and size $z = 40$. Binding affinities were reported in kcal mol^{-1}. After docking, the receptor–ligand interactions were analyzed using BIOVIA Discovery Studio Visualizer 2024. The analysis provided 2D and 3D visualizations, enabling the detailed examination of interaction patterns within the ligand–protein complexes.

Molecular dynamics

Molecular dynamics (MD) simulations were performed on both the apo form of PTP-1B (PDB ID: 2QBP) and its complexes with five lead compounds using GROMACS 2024.2. The CHARMM27 force field was used for protein topology generation, while water molecules were described using the TIP3P model. Ligand topologies were obtained from the CGenFF web server and converted into GROMACS-compatible formats using a Python script provided by the MacKerell lab. Each system was placed in a dodecahedral box, with a minimum distance of 1.0 nm between the solute and the box boundaries. After solvation and neutralization with Na^+ ions, energy minimization was carried out using the steepest descent algorithm until the maximum force fell below 100 kJ mol^{-1} nm^{-1}. Equilibration was performed in two successive 100 ps phases: an NVT ensemble at 300 K using the V-rescale thermostat, followed by an NPT ensemble at 1 bar using the Parrinello–Rahman barostat. Long-range electrostatic interactions were treated using the particle mesh Ewald (PME) method, while all bonds involving hydrogen atoms were constrained using the LINCS algorithm. A 100 ns production run was subsequently performed, with trajectory frames saved every 10 ps. The resulting trajectories were used for further analysis, including binding free energy calculations. Binding free energies (ΔG_{bind}) were calculated using the MM/GBSA method implemented in gmx_MMPBSA 1.6.3, based on snapshots extracted from the final 20 ns of the simulation. The total binding free energy was calculated as the sum of ΔE_{MM} and ΔG_{solv} using the GB-OBC2 implicit solvent model at a salt concentration of 0.15 M. Per-residue energy decomposition analysis was performed to identify key residues contributing to ligand binding within the PTP-1B active site.

In silico ADME and toxicity prediction methods

The *in silico* ADME predictions of the three compounds were performed using the ADME SwissADME web tool (https://www.swissadme.ch/, accessed August 6, 2025) and ADMETlab 3.0 (https://admetlab3.scbdd.com/, accessed August 6, 2025). The SMILES format of each compound was used to compute key physicochemical properties and was evaluated by ChemDraw 21.0. The compounds were also analysed for their pharmacokinetic profiles, including gastrointestinal absorption, $\log K_p$ (skin permeation), and interaction with cytochrome P450. The *in silico* toxicity predictions of three compounds were made using the Tox prediction web tool (https://tox.charite.de/protox3/index.php?site=compound_input, accessed 6th August 2025). The toxicity predictions included classification into toxicity categories and the estimation of the median lethal dose (LD_{50}) and interaction between compounds and biological targets critical to key physiological processes, offering valuable insights into the safety and potential risks of these compounds.

Author contributions

Conceptualization: Le Viet Ha Tran and Huu Canh Vo; isolation and identification: Minh Canh Nguyen, Thanh-Tung Phan, and Nguyen Tri Quang; bioassay: Le Viet Ha Tran; computational studies: Linh Tran, Quang-Minh Mai, and Phuc Tran Huu Le; writing – original draft preparation: Huu Canh Vo; writing – review and editing: Huynh Nguyen Khanh Tran; supervision: Khac-Minh Thai; and project administration: Linh Tran. All authors have read and agreed to the published version of the manuscript.

Conflicts of interest

The authors declare no competing financial interests.

Data availability

The data that support the findings of this study are available in the supplementary information (SI). Supplementary information: spectral data of isolated compounds. See DOI: https://doi.org/10.1039/d6ra02679f.

Acknowledgements

This research is funded by Vietnam National Foundation for Science and Technology Development (NAFOSTED) under grant number 108.06-2025.114.

References

1 R. Mahajan and M. Chopda, *Pharmacogn. Rev.*, 2009, **3**, 320.
2 P. Oudhia, 2003, https://www.botanical.com/site/column_poudhia/250_brahmadandi.html.
3 Q.-H. Gao, C.-S. Wu and M. Wang, *J. Agric. Food Chem.*, 2013, **61**, 3351–3363.
4 F. Vahedi, M. F. Najaf and K. Bozari, *Cytotechnology*, 2008, **56**, 105–111.
5 N. M. N. MinKyun, A. R. A. RenBo, L. S. Lee, S.-M. Lee, H. N. Hong, N.-D. Hong, Y. J. Yoo, J.-K. Yoo, L. C. L. ChanBok, K. J. Kim and K.-H. Bae, *Korean J. Pharmacogn.*, 2001, **32**, 108–115.
6 L. Huang, W. Ye, B. Cai, D. Li, J. Liu and M. Liu, *Chin. J. Chin. Mater. Med.*, 1990, **15**, 115–117.
7 X. Shen, Y. Tang, R. Yang, L. Yu, T. Fang and J.-A. Duan, *J. Ethnopharmacol.*, 2009, **122**, 555–560.
8 S. M. Lee, B. S. Min, C.-G. Lee, K.-S. Kim and Y. H. Kho, *Planta Med.*, 2003, **69**, 1051–1054.
9 P. Dzubak, M. Hajduch, D. Vydra, A. Hustova, M. Kvasnica, D. Biedermann, L. Markova, M. Urban and J. Sarek, *Nat. Prod. Rep.*, 2006, **23**, 394–411.
10 Q.-C. Liu, T.-T. Guo, L. Zhang, Y. Yu, P. Wang, J.-F. Yang and Y.-X. Li, *Bioorg. Med. Chem.*, 2013, **63**, 511–522.
11 A. Alqahtani, K. Hamid, A. Kam, K. Wong, Z. Abdelhak, V. Razmovski-Naumovski, K. Chan, K. M. Li, P. W. Groundwater and G. Q. Li, *Curr. Med. Chem.*, 2013, **20**, 908–931.
12 P.-Y. Gao, M. Wang, X.-G. Liu, Y.-X. Gao, J.-L. Li, Z.-X. Zhang, H.-W. Lin and S.-J. Song, *RSC Adv.*, 2016, **6**, 2431–2435.
13 S.-S. Lee, W.-C. Su and K. C. Liu, *J. Nat. Prod.*, 1991, **54**, 615–618.
14 A. Kundu, B. Barik, D. Mondal, A. Dey and A. Banerji, *Phytochemistry*, 1989, **28**, 3155–3158.
15 N. Q. Chien, N. V. Hung, B. D. Santarsiero, A. D. Mesecar, N. M. Cuong, D. D. Soejarto, J. M. Pezzuto, H. H. Fong and G. T. Tan, *J. Nat. Prod.*, 2004, **67**, 994–998.
16 L. Pohjala, S. Alakurtti, T. Ahola, J. Yli-Kauhaluoma and P. Tammela, *J. Nat. Prod.*, 2009, **72**, 1917–1926.
17 W. Seebacher, N. Simic, R. Weis, R. Saf and O. Kunert, *Magn. Reson. Chem.*, 2003, **41**, 636–638.
18 H. Sun, W.-S. Fang and C. Hu, *J. Asian Nat. Prod. Res.*, 2008, **10**, 271–276.
19 S. Liang, E. Tran, X. Du, J. Dong, H. Sudholz, H. Chen, Z. Qu, N. D. Huntington, J. J. Babon and N. J. Kershaw, *Nat. Chem. Biol.*, 2023, **14**, 4524.
20 W. Herz, P. Santhanam and I. Wahlberg, *Phytochem.*, 1972, **11**, 3061–3063.
21 M. S. Ali, S. A. Ibrahim, S. Jalil and M. I. Choudhary, *Phytother. Res.*, 2007, **21**, 558–561.
22 K. W. Woo, J. Y. Han, S. U. Choi, K. H. Kim and K. R. Lee, *Nat. Prod. Sci.*, 2014, **20**, 71–75.
23 A. Yagi, N. Okamura, Y. Haraguchi, K. Noda and I. Nishioka, *Chem. Pharm. Bull.*, 1978, **26**, 1798–1802.
24 T. Furuya, Y. Orihara and C. Hayashi, *Phytochem.*, 1987, **26**, 715–719.
25 H. C. Pitot, *Cancer*, 1993, **72**, 962–970.
26 R. J. Andrade, N. Chalasani, E. S. Björnsson, A. Suzuki, G. A. Kullak-Ublick, P. B. Watkins, H. Devarbhavi, M. Merz, M. I. Lucena and N. Kaplowitz, *Nat. Rev. Dis. Primers*, 2019, **5**, 58.
27 C. P. K. Vrundha and T. D. Thomas, *J. Genet. Eng. Biotechnol.*, 2023, **21**, 70.

28 D. T. Loi, *Medicinal Plants and Drugs from Vietnam*, Publisher of Medicine, Hanoi, 2006.
29 P. H. Nguyen, T. T. Dao, J. Kim, D. T. Phong, D. T. Ndinteh, J. T. Mbafor and W. K. J. B. Oh, *Bioorg. Med. Chem.*, 2011, **19**, 3378–3383.
30 B. Na, P.-H. Nguyen, B.-T. Zhao, Q.-H. Vo, B. S. Min and M. H. Woo, *Pharm. Biol.*, 2016, **54**, 474–480.
31 H. Kurihara, J. Ando, M. Hatano and J. Kawabata, *Bioorg. Med. Chem. Lett.*, 1995, **5**, 1241.
32 H. C. Vo, T. H. Long, V. H. La, Q. T. Le, M. C. Nguyen, D. T. Le, T. D. L. Nguyen, T.-T. Phan, N. T. T. Duong and Q. T. That, *RSC advances*, 2025, **15**, 50103–50110.
33 S. Liang, E. Tran, X. Du, J. Dong, H. Sudholz, H. Chen, Z. Qu, N. D. Huntington, J. J. Babon and N. J. Kershaw, *Nat. Chem. Biol.*, 2023, **14**, 4524.